Available online at www.sciencedirect.com
SCIENCE DIRECT®
Composites Science and Technology 65 (2005) 2492–2499
COMPOSITES SCIENCE AND TECHNOLOGY
www.elsevier.com/locate/compscitech

Mechanical and magnetic properties of metal fibre networks, with and without a polymeric matrix

T.W. Clyne *, A.E. Markaki, J.C. Tan

Department of Materials Science and Metallurgy, Cambridge University, Pembroke Street, Cambridge CB2 3QZ, UK

Received 26 May 2005; accepted 26 May 2005
Available online 18 August 2005

Abstract

Bonded networks of metal fibres are highly porous, permeable materials, which often exhibit relatively high strength. Material of this type has been produced, using melt-extracted ferritic stainless steel fibres, and characterised in terms of fibre volume fraction, fibre segment (joint-to-joint) length and fibre orientation distribution. Young's moduli and yield stresses have been measured. The behaviour when subjected to a magnetic field has also been investigated. This causes macroscopic straining, as the individual fibres become magnetised and tend to align with the applied field. The modeling approach of Markaki and Clyne, recently developed for prediction of the mechanical and magneto-mechanical properties of such materials, is briefly summarised and comparisons are made with experimental data. The effects of filling the inter-fibre void with compliant (polymeric) matrices have also been explored. In general the modeling approach gives reliable predictions, particularly when the network architecture has been characterised using X-ray tomography.

Keywords: Metal fibres; Ferromagnetism; Elastic constants; Magneto-mechanical actuation; X-ray tomography

1. Introduction

There is current interest [1–9] in materials made by bonding together slender metallic members, such as fibres, wires, rods, ribbons etc. This can be done by welding, brazing, sintering or adhesive bonding. An illustrative fibre architecture is shown in Fig. 1. Such network materials usually incorporate high void contents (~40–98%) and can exhibit interesting properties. Of course, the mechanical efficiency of various strut assemblies, such as trusses, is well known, but translation of such concepts into design of porous materials (or composites) is still evolving. Furthermore, the high surface-to-mass ratio of bonded fibre networks, coupled with the relatively good environmental stability of metals, means that they can be attractive in terms of transport phenomena characteristics, leading to applications involving heat transfer, filtration, catalyst support, acoustic damping etc. When the fibres are ferromagnetic, there is potential for exercising control over fibre orientation distributions during processing via applied magnetic fields and there is also scope for the magnetic induction of mechanical strain in the material (see below).

A recently introduced idea [10,11], with potential for the development of actuation applications, is based on the way in which an assembly of ferromagnetic fibres is expected to deform under the influence of an applied magnetic field, as individual fibres tend to align with the field. This effect is illustrated schematically in Fig. 2. It has been suggested [10] that this effect could be utilised to stimulate bone growth, since bone tissue growing into such a porous array would be strained when a magnetic field was applied, with potential physiological benefits. An analytical model has been presented [10,11] for

* Corresponding author. Tel.: +44 1223 334332; fax: +44 1223 334567.
E-mail address: twc10@cam.ac.uk (T.W. Clyne).

0266-3538/$ - see front matter © 2005 Published by Elsevier Ltd.
doi:10.1016/j.compscitech.2005.05.037

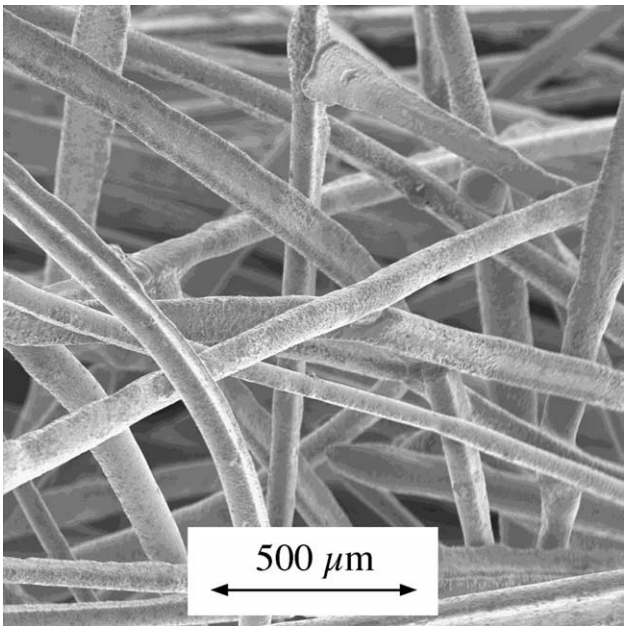

Fig. 1. Scanning electron micrograph of a bonded fibre network material, made by brazing short ferritic stainless steel fibres.

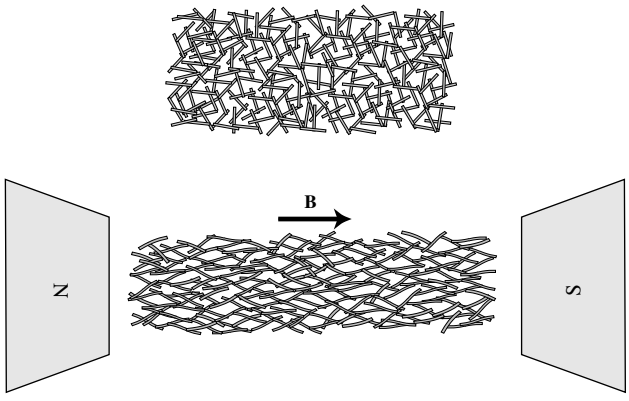

Fig. 2. Schematic representation of how a bonded network of randomly oriented ferromagnetic fibres will deform in a magnetic field.

prediction of the induced deformation, together with experimental validation for single fibres and for small 4-fibre assemblies.

In the present paper, a brief overview is presented of the mechanical and magneto-mechanical characteristics of non-periodic ferromagnetic fibre networks, as a function of the fibre architecture, and the presence or absence of a (relatively compliant) matrix in the interstitial space. Some relevant information about material production, testing procedures and model development is supplied in earlier papers [10,11].

2. An analytical framework based on fibre bending

A simple analytical model has been developed by Markaki and Clyne [10,11], based on the bending of individual fibre segments (sections between joints). It is assumed that the deflections and strains exhibited by the network arise predominantly from this type of deformation, which is expected to be acceptable provided the segments are relatively slender.

2.1. Elastic mechanical loading

The loading situation is depicted schematically in Fig. 3(a), focussing on the elastic deformation exhibited by a single fibre segment, lying with its axis at an angle θ to the loading direction. When a uniaxial stress is applied, a force W acts on it in the loading direction, generating a bending moment. Application of standard cantilever bending mechanics leads to expressions for the axial and transverse deflections, as a function of the applied stress σ (assuming uniform partitioning of the load to all fibres)

$$\Delta z = \frac{4\sigma L^3 \sin^2\theta}{3E_f f D^2}, \tag{1}$$

$$\Delta r = \frac{4\sigma L^3 \sin\theta\cos\theta}{3E_f f D^2}. \tag{2}$$

The macroscopic deflection in the loading direction, and hence the overall strain, can be obtained by summing the contributions from the deflections of individual fibres. Doing this in a rigorous manner is clearly complex, since the deflections exhibited by individual fibre segments will be influenced by the configuration of neighbouring segments. However, if these interactions are neglected, then the net strain can be obtained by simple integration. If the fibre orientation distribution is isotropic, so that it exhibits a $\sin\theta$ probability about any given axis, then the axial strain is given by

$$\varepsilon_z = \frac{\Delta Z}{Z} = \frac{\int_0^{\pi/2} \Delta z \sin\theta \,\mathrm{d}\theta}{\int_0^{\pi/2} z \sin\theta \,\mathrm{d}\theta} = \frac{\int_0^{\pi/2} \frac{4\sigma L^3 \sin^3\theta}{3E_f f D^2} \,\mathrm{d}\theta}{\int_0^{\pi/2} \left(\frac{L}{2}\cos\theta\right) \sin\theta \,\mathrm{d}\theta}, \tag{3}$$

$$\therefore \varepsilon_z = \left(\frac{8\sigma}{3E_f f}\right)\left(\frac{L}{D}\right)^2 \frac{\int_0^{\pi/2} \sin^3\theta \,\mathrm{d}\theta}{\int_0^{\pi/2} \cos\theta \sin\theta \,\mathrm{d}\theta}$$

$$= \left(\frac{8\sigma}{3E_f f}\right)\left(\frac{L}{D}\right)^2 \frac{2/3}{1/2} = \left(\frac{32\sigma}{9E_f f}\right)\left(\frac{L}{D}\right)^2, \tag{4}$$

so the Young's modulus of the network is given by

$$E_a = \frac{9E_f f}{32\left(\frac{L}{D}\right)^2}. \tag{5}$$

The form of this prediction may be compared with that given by Gibson and Ashby [12] for a similar type of material. This is also based on beam deflections (3-point bending under a normal load, rather than the connected pair of inclined cantilevers assumed in the present model), but the geometry is more constrained. Assuming simply supported cylindrical beams lying parallel or

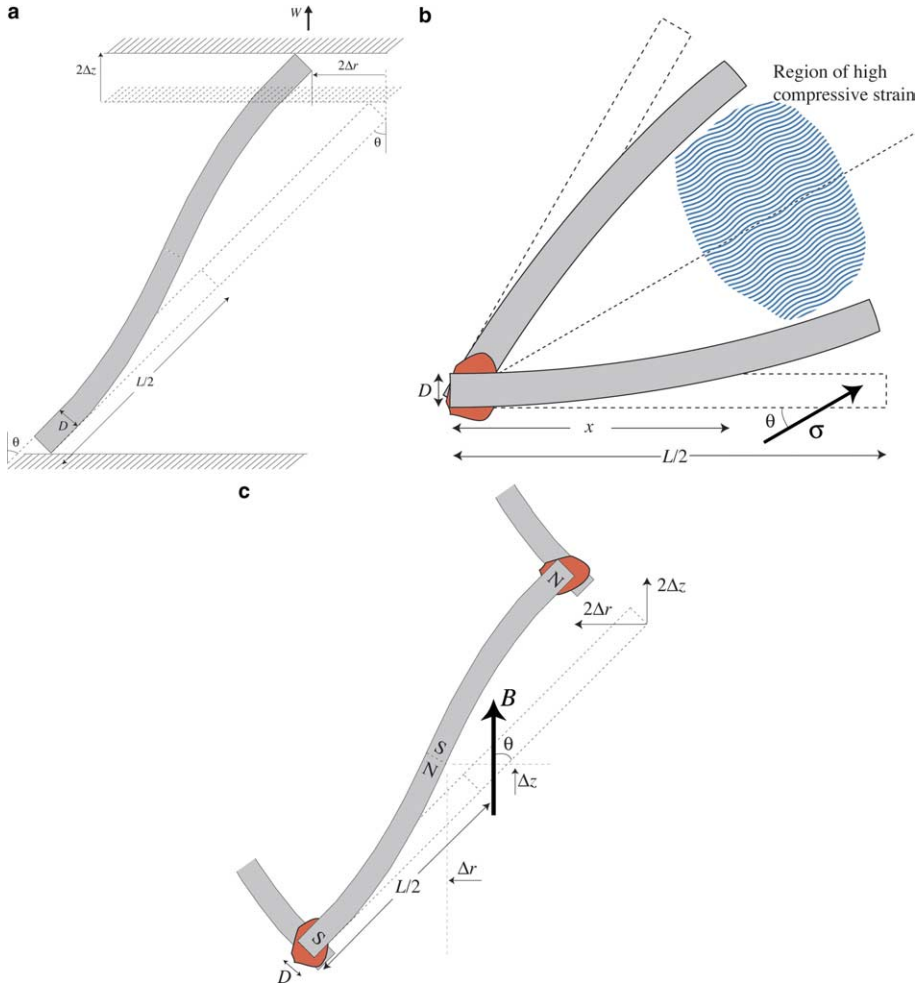

Fig. 3. Schematic representations of (a) deflection of a fibre segment within a network, under the influence of an applied force, W, (b) generation of strain within a surrounding environment and (c) deflection of a (ferromagnetic) fibre under the influence of a magnetic field.

normal to the applied load, the Young's modulus predicted by the Gibson and Ashby model can be expressed in terms of L and D as follows:

$$E_a = \frac{3\pi E_f}{4\left(\frac{L}{D}\right)^4}. \tag{6}$$

Similarly, the transverse strain is given by

$$\varepsilon_r = \frac{\Delta R}{R} = \frac{\int_0^{\pi/2} \Delta r \sin\theta \, d\theta}{\int_0^{\pi/2} r \sin\theta \, d\theta}$$

$$= \left(\frac{8\sigma}{3E_f f}\right)\left(\frac{L}{D}\right)^2 \frac{\int_0^{\pi/2} \sin^2\theta \cos\theta \, d\theta}{\int_0^{\pi/2} \sin^2\theta \, d\theta}, \tag{7}$$

$$\therefore \varepsilon_r = \left(\frac{8\sigma}{3E_f f}\right)\left(\frac{L}{D}\right)^2 \frac{1/3}{\pi/4} = \left(\frac{32\sigma}{9\pi E_f f}\right)\left(\frac{L}{D}\right)^2. \tag{8}$$

The Poisson ratio, v ($=\varepsilon_r/\varepsilon_z$) is thus predicted to have a constant value of $1/\pi(\sim 0.32)$, independent of the fibre volume fraction and fibre segment aspect ratio. Since the material is isotropic, E_a and v together fully define the elastic behaviour. Of course, if the actual distributions of θ and L/D are known, then Eqs. (3) and (7) can be (numerically) integrated using these functions – see Section 5.

2.2. Onset of inelastic behaviour

The stresses within a cantilever beam are known, so it is a simple matter to predict the applied load at which the peak stress within the system will reach the yield stress of the fibre material. The maximum local stress will occur at the fibre surface, at the position along the beam where the bending moment reaches a peak (i.e., adjacent to the joints)

$$\sigma_{f,max} = \frac{D}{2}\frac{M}{I} = \frac{D}{2}\frac{W\sin\theta(L/2)}{(\pi D^4/64)}. \tag{9}$$

On setting this stress equal to the fibre yield stress, $\sigma_{f,Y}$, and substituting for W, an estimate can be obtained of the applied stress for the onset of yielding.

$$\sigma_{a,Y} = \sigma_{f,Y}\frac{f}{8\left(\frac{L}{D}\right)}. \tag{10}$$

2.3. Effect of the presence of an environment (matrix)

The behaviour is modified when material is introduced into the inter-fibre space. If this material has a much lower stiffness than the fibre, then this modification can readily be analysed, since the form of the deflection–distance relationship along the length of the fibre is then expected to be the same (assuming that the matrix is elastically homogeneous and isotropic), although the deflections will clearly be reduced. By comparing deflections with and without a matrix, it can be shown that the Young's modulus E_c of a fibre network surrounded by a medium with finite stiffness (i.e., a composite) is given by

$$E_c = \frac{9E_f f}{32\left(\frac{L}{D}\right)^2 Q}, \tag{11}$$

where Q is a strain reduction factor, which is a function of the environment/fibre stiffness ratio and the fibre segment aspect ratio. The Poisson ratio is predicted to be unaffected by the presence of the matrix. It should be borne in mind that the model is only expected to be valid in cases where $E_e \ll E_f$ and $(L/D) > \sim 3$, where the subscript "e" represents the environment (or matrix).

2.4. Magnetic loading

A magnetic load is generated by the application of a uniaxial magnetic field. This will always tend to generate an axial tensile strain in the fibre network, as a consequence of individual fibres becoming magnetised along their length and hence tending to line up parallel to the applied field see Figs. 2 and 3(c). Any effect on the net field experienced by an individual fibre, arising from the magnetisation of neighbouring fibres, is assumed to be small. The torque (bending moment) acting on a magnetic dipole lying in a magnetic field B generates net deflections in a similar manner to an applied mechanical load, leading to expressions for the deflections parallel and normal to the applied field, at a distance x along the length of the fibre

$$\frac{\Delta z}{z} = \frac{\delta \sin\theta}{x\cos\theta} = \frac{8M_s B \sin\theta\tan\theta}{3E_f}\left[3\left(\frac{x}{L}\right) - \left(\frac{x}{L}\right)^2\right]\left(\frac{L}{D}\right)^2, \tag{12}$$

$$\frac{\Delta r}{r} = \frac{-\delta\cos\theta}{x\sin\theta} = \frac{-8M_s B\cos\theta}{3E_f}\left[3\left(\frac{x}{L}\right) - \left(\frac{x}{L}\right)^2\right]\left(\frac{L}{D}\right)^2, \tag{13}$$

where M_s is the saturation magnetisation. The broad validity of these expressions has been confirmed experimentally [10] by comparing measured and predicted deflections for single pieces of wire and for small welded assemblies.

The overall extension parallel to the applied field can be expressed by considering the displacements of a set of fibre mid-points (see Fig. 3(c))

$$\frac{\Delta Z}{Z} = \frac{\int_0^{\pi/2}\Delta z\sin\theta\,d\theta}{\int_0^{\pi/2} z\sin\theta\,d\theta} = \frac{\int_0^{\pi/2}\frac{8M_s B}{3E_f D^2}\sin^2\theta\left(3\left(\frac{L}{2}\right)^3 - \left(\frac{L}{2}\right)^3\right)\sin\theta\,d\theta}{\int_0^{\pi/2}\left(\frac{L}{2}\cos\theta\right)\sin\theta\,d\theta},$$

$$\therefore \frac{\Delta Z}{Z} = \frac{\frac{2M_s BL}{3E_f}\left(\frac{L}{D}\right)^2\int_0^{\pi/2}\sin^3\theta\,d\theta}{\frac{L}{4}} = \left(\frac{16M_s B}{9E_f}\right)\left(\frac{L}{D}\right)^2. \tag{14}$$

The concept of "*magnetic* stiffness" of a bonded fibre array, S_a $(=B/\varepsilon_z)$ may now be introduced. This represents the applied field required to generate unit elastic strain, in an analogous manner to the Young's modulus representing the applied stress needed to generate unit elastic strain.

$$S_a = \frac{9E_f}{16M_s\left(\frac{L}{D}\right)^2}. \tag{15}$$

The transverse contraction is similarly derived:

$$\frac{\Delta R}{R} = \frac{\int_0^{\pi/2}\Delta r\sin\theta\,d\theta}{\int_0^{\pi/2} r\sin\theta\,d\theta} = \frac{\int_0^{\pi/2}\frac{-8M_s B}{3E_f D^2}\sin\theta\cos\theta\left(3\left(\frac{L}{2}\right)^3 - \left(\frac{L}{2}\right)^3\right)\sin\theta\,d\theta}{\int_0^{\pi/2}\left(\frac{L}{2}\sin\theta\right)\sin\theta\,d\theta},$$

$$\therefore \frac{\Delta R}{R} = \frac{\frac{-2M_s BL}{3E_f}\left(\frac{L}{D}\right)^2\int_0^{\pi/2}\sin^2\theta\cos\theta\,d\theta}{L\left(\frac{\pi}{8}\right)} = \left(\frac{-16M_s B}{9\pi E_f}\right)\left(\frac{L}{D}\right)^2. \tag{16}$$

3. Mechanical properties

3.1. Elastic constants

Predicted relative stiffnesses are shown in Fig. 4, as a function of fibre segment aspect ratio, for the Gibson and Ashby model (Eq. (6)) and for the isotropic fibre network model (Eq. (5)), with three fibre volume fractions. Also shown are measured stiffness values for free-standing bonded fibre arrays with different f and L/D values. (These fibre segment aspect ratios for the bonded fibre arrays were estimated from SEM micrographs, such as the one shown in Fig. 1.) The Gibson and Ashby model predicts a sharper fall in stiffness with increasing L/D than the Markaki and Clyne model. However, increases in L/D would often be accompanied by reductions in fibre content, f,

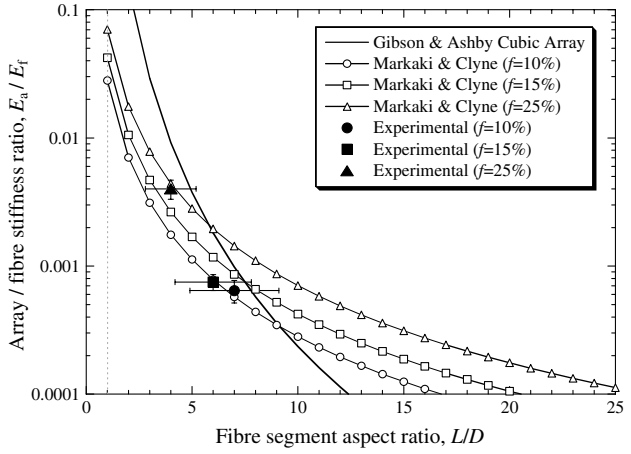

Fig. 4. Comparison between theory (Eq. (5)) and experiment for the relative stiffness of fibre networks, with different fibre volume fractions. Also shown are predictions from the Gibson and Ashby model for a cubic array fibres (Eq. (6)), for which the fibre volume fraction is related to the segment aspect ratio.

making the effective plot for the Markaki and Clyne model somewhat steeper than the individual curves.

3.2. Yielding behaviour

The stress at the onset of yielding, predicted by Eq. (10), is plotted in Fig. 5 as a function of L/D ratio, for networks with different fibre contents. Also included on this plot are measured values, taken as stress levels at the onset of the plateau regime in the stress–strain curve. The yield strength of the fibre ($\sigma_{f,Y} = 1000$ MPa) was obtained from single fibre testing [7]. It can be seen that the experimental data are broadly consistent with predictions from the model.

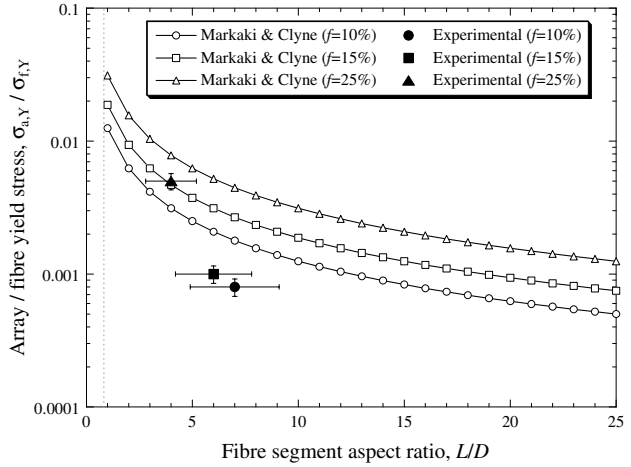

Fig. 5. Predicted stress at the onset of inelastic behaviour of fibre arrays, as a function of segment aspect ratio, for different fibre volume fractions. Also shown are corresponding experimental data.

4. Magneto-mechanical characteristics

The response to the application of a magnetic field of both free-standing fibre networks and those infiltrated with rubber or resin is illustrated in Fig. 6. The plots show relative length changes of the specimens, as a function of the applied magnetic field. The field was ramped up and down, with a maximum value of about 1.2 Tesla. Length changes approaching 0.2% were recorded for the free-standing fibre array (Fig. 6(a)) and the array infiltrated with rubber (Fig. 6(b)), whereas for the resin-impregnated array (Fig. 6(b)), the straining was barely detectable. The latter is unsurprising, since the strains are reduced as the constraint imposed by the surrounding material increases. The rate of strain increase drops at higher field strengths. This is probably a geometric effect, since the fibre deflections will approach saturation at high fields and the predicted deflections refer only to the low strain regime. Furthermore, it can also be seen that there is some hysteresis, with the induced length change not being entirely reversible on reducing

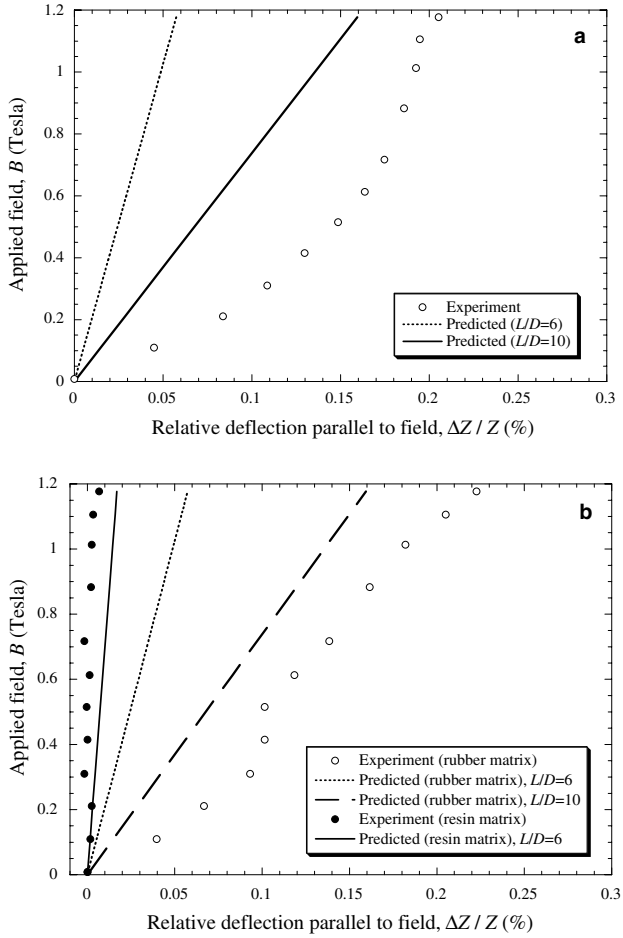

Fig. 6. Comparison between theory and experiment for the change in length as a function of magnetic field strength for (a) a free-standing fibre network and (b) fibre networks infiltrated with rubber or resin.

the applied field. This may be due to formation of fibre entanglements, which persist after removal of the field. This effect appears more pronounced for the rubber-impregnated array, which may be attributable to creep deformation of the rubber.

Comparison between measured and predicted changes shows that, for the non-impregnated and the rubber-impregnated arrays, the measured deflections are larger than those predicted by the model. While close agreement with experiment is not really expected here, since in reality the deformation behaviour of a fibre network is expected to be complex, it is important to note that these predictions are very sensitive to the segment aspect ratio. This is illustrated in Fig. 6, which shows predicted shape changes as a function of the applied magnetic field, for two segment aspect ratios. The value of 6 used for the prediction was estimated from micrographs such as those shown in Fig. 1. Predictions are also shown for a segment aspect ratio of 10, since it is possible that not all the fibres are bonded at their cross-over points.

5. Characterisation of network architecture

It is clear that systematic quantitative study of fibre network materials requires accurate and reliable characterisation of their architecture. The analysis and predictions presented earlier are crude in this respect, with isotropy being assumed and fibre segment lengths being estimated visually from micrographs. In fact, it is well known that such networks are rarely isotropic, although, depending on the manufacturing technique, they are often transversely isotropic. Such characterisation is now being undertaken, using the technique of computed X-ray micro-tomography [13,14]. An illustrative example is given here. Full details are presented elsewhere [15]. Standard software packages are now available which create visualisations of the structure from tomographic data. Fig. 7 shows such a visualisation, for a network material composed of 5 mm long ferritic stainless steel (446) fibres, sintered for 5 h at 1200 °C, after being gently compressed (manually) in the axial direction within a tube. The relative density (fibre volume fraction) is about 10%. The fibres were produced by a melt extraction process and have a cross section with an equivalent diameter of about 60 micron. Most fibre sections are actually somewhat flattened or crescent-shaped and this can be seen in the visualisation.

A skeletonisation algorithm has been employed [15], allowing fibre segments to be vectorised from tomography data of this type, and this has allowed fibre orientation distributions to be obtained for these materials. Fig. 8 shows the orientation distribution for the material illustrated in Fig. 7. It can be seen that in this case there

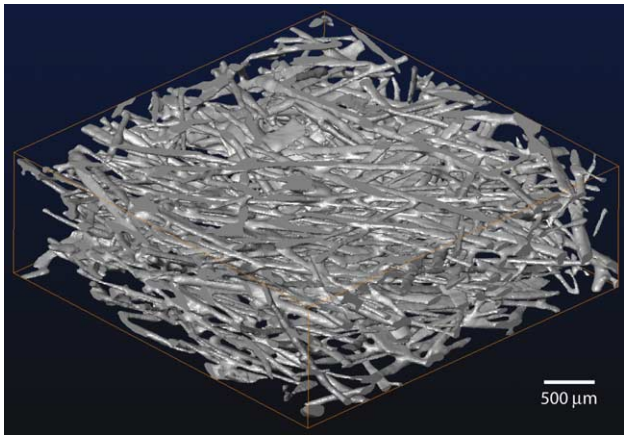

Fig. 7. Visualisation of the architecture of a fibre network material, obtained by computed X-ray micro-tomography.

is a marked tendency for the fibres to lie at relatively large angles to the unique (pressing) direction. This is readily explicable, although the strength of the effect is expected to depend on the fibre length, and perhaps also on fibre yielding and work-hardening characteristics, as well as on the compression pressure.

It is now possible to predict the elastic constants of this material, retaining the assumptions about uniform partitioning of the load between individual fibres, and neglect of local constraint geometries, but utilising the actual distribution of fibre orientation in the integration procedure. Since the skeletonisation algorithm allows evaluation of fibre segment lengths, as well as orientations, it is possible for this distribution to be included in the integration, and even for coupling between them to be taken into account, but for present purposes it is assumed that all fibre segments are of the (measured) average length, which is about 540 micron, so that L/D is about 9.

The integration required to give the predicted strain can now be written

$$\varepsilon_z = \frac{\Delta Z}{Z} = \frac{\int_0^{\pi/2} \Delta z P(\theta)\,\mathrm{d}\theta}{\int_0^{\pi/2} z P(\theta)\,\mathrm{d}\theta} = \frac{\int_0^{\pi/2} \frac{4\sigma L^3 \sin^2\theta}{3E_f f D^2} P(\theta)\,\mathrm{d}\theta}{\int_0^{\pi/2} \left(\frac{L}{2}\cos\theta\right) P(\theta)\,\mathrm{d}\theta} \tag{17}$$

$$\therefore \varepsilon_z = \left(\frac{8\sigma}{3E_f f}\right)\left(\frac{L}{D}\right)^2 \frac{\int_0^{\pi/2} \sin^2\theta P(\theta)\,\mathrm{d}\theta}{\int_0^{\pi/2} \cos\theta(\theta)\,\mathrm{d}\theta}$$

$$= \left(\frac{8\sigma}{3E_f f}\right)\left(\frac{L}{D}\right)^2 \frac{\sum_i^n \sin^2\theta_i P(\theta_i)\Delta\theta_i}{\sum_i^n \cos\theta_i P(\theta_i)\Delta\theta_i}, \tag{18}$$

where the segment orientation distribution, $P(\theta_i)$, is given by

$$P(\theta_i) = \frac{1}{\Delta\theta_i} \cdot \frac{N_{\theta_i}}{\sum_i^n N_{\theta_i}}, \tag{19}$$

where N_{θ_i} is the number of fibres inclined at an angle θ_i (i.e., within a bin of width of $\Delta\theta_i$, centred at θ_i).

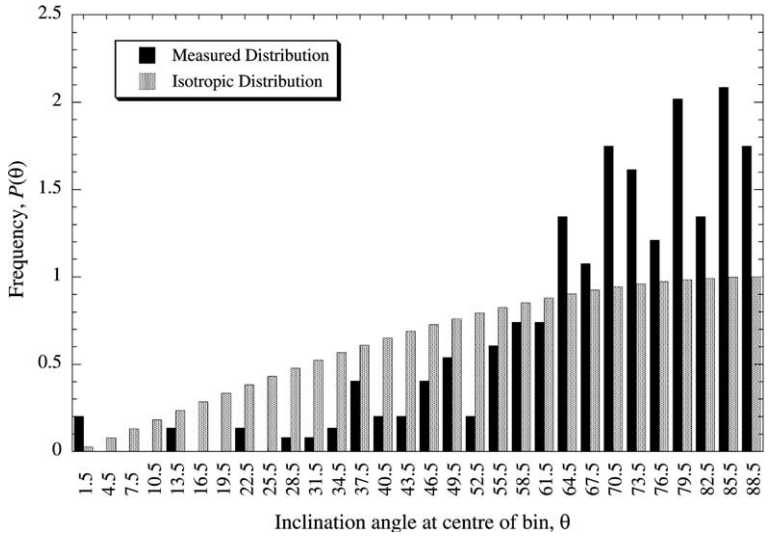

Fig. 8. Distribution of inclination angles for the structure visualised in Fig. 7, obtained from the tomography data after skeletonisation of the network and vectorisation of the fibre segments.

$$\therefore \varepsilon_z = \left(\frac{8\sigma}{3E_f f}\right)\left(\frac{L}{D}\right)^2 \frac{\frac{\sum_i^n N_{\theta_i}\sin^2\theta_i}{\sum_i^n N_{\theta_i}}}{\frac{\sum_i^n N_{\theta_i}\cos\theta_i}{\sum_i^n N_{\theta_i}}}$$

$$= \left(\frac{8\sigma}{3E_f f}\right)\left(\frac{L}{D}\right)^2 \frac{\sum_i^n N_{\theta_i}\sin^2\theta_i}{\sum_i^n N_{\theta_i}\cos\theta_i}. \quad (20)$$

The axial Young's modulus of the fibre array, E_a ($=\sigma/\varepsilon_z$), is therefore given by

$$E_{ax} = \frac{3E_f f}{8\left(\frac{L}{D}\right)^2} \frac{\sum_i^n N_{\theta_i}\cos\theta_i}{\sum_i^n N_{\theta_i}\sin^2\theta_i}. \quad (21)$$

Similarly, the transverse Young's modulus is given by

$$E_{tr} = \frac{3E_f f}{8\left(\frac{L}{D}\right)^2} \frac{\sum_i^n N_{\theta_i}\cos\left(\frac{\pi}{2}-\theta_i\right)}{\sum_i^n N_{\theta_i}\sin^2\left(\frac{\pi}{2}-\theta_i\right)} \quad (22)$$

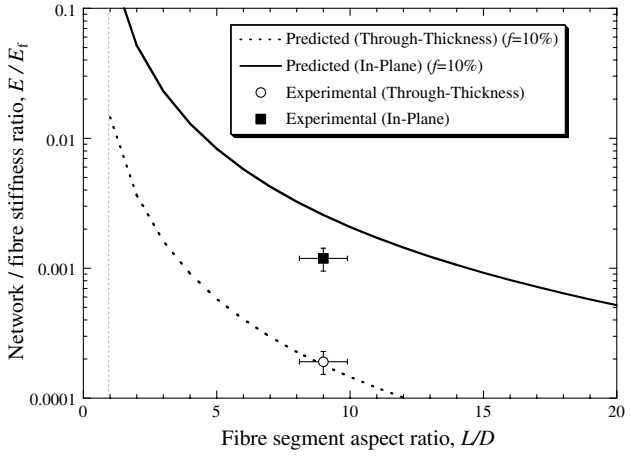

Fig. 9. Predicted dependence of network stiffness on fibre segment aspect ratio, in axial (through-thickness) and transverse (in-plane) directions, based on the orientation distribution data shown in Fig. 8. Also shown are measured stiffnesses in these two directions.

Fig. 9 shows a comparison between predictions obtained using these two equations and experimentally measured stiffness values for this material, plotted at the L/D value estimated from the tomography data ($L/D = 9$). While agreement is not perfect, there is a good level of consistency, not only for the anisotropy (ratio of stiffness in axial and transverse directions), but also in terms of the absolute values. This suggests that the rather crude assumptions made about load partitioning and local constraint effects are not too unrealistic, although these measurements relate only to a single material and more comprehensive studies are clearly required.

6. Conclusions

This paper presents an overview of recent developments concerning network materials composed of bonded (ferromagnetic) metal fibres, with or without a compliant (polymeric) matrix. A simple analytical framework for prediction of mechanical and magneto-mechanical properties, originated by Markaki and Clyne, is briefly outlined here. The following detailed points may be noted.

(1) Simple analytical models are described, based on deformation being dominated by bending of individual fibres. These models are applicable to cases in which the fibre segments (between joints) are relatively slender and any matrix present is much more compliant than the fibre material. Net dimensional changes are obtained via a simple integration procedure, summing the deflections which would be exhibited by individual fibres if they were free-standing.

(2) An expression has been derived for the Young's modulus, as a function of fibre segment aspect ratio, L/D, and fibre volume fraction, f. The form of this prediction is similar to that of a previously developed expression (Gibson and Ashby model) based on a regular, orthogonal set of fibres, except that L/D and f can be independently specified in the current model and the predicted dependence on aspect ratio is rather less sharp.
(3) The effect of the presence of a (compliant) matrix has been simulated via some crude assumptions about how its presence will inhibit fibre bending. This leads to an expression for a "strain reduction factor", dependent on L/D and the matrix/fibre stiffness ratio.
(4) The onset of plastic deformation has also been modelled, by comparing peak stresses within the fibres with the nominal yield stress of the fibre material.
(5) Predictive equations are presented for the elastic deformation induced by the imposition of a magnetic field. The concept of a "magnetic stiffness", S, is introduced, analogous to a Young's modulus, E, in the sense that it is the applied magnetic field needed to induce unit elastic strain, whereas E is the applied stress needed to induce unit elastic strain. The expression for S incorporates the saturation magnetisation of the fibre material, as well as the fibre Young's modulus and the fibre segment aspect ratio.
(6) Comparisons between theory and experiment are presented for Young's modulus, yield stress and magnetic stiffness, based on the assumption of an isotropic fibre orientation distribution. Fairly good agreement is observed, but in practice many network materials are likely to exhibit pronounced anisotropy and in such cases quantification of the fibre architecture is essential for reliable modelling. This quantification is best done using computed X-ray tomography and a preliminary comparison is presented between measured (axial and transverse) stiffness and predictions based on a fibre orientation distribution obtained in this way. This comparison is encouraging and suggests that the proposed modeling approach, in conjunction with tomography studies, should prove a useful tool for further development of fibre network materials.

Acknowledgements

Financial support for this work has come from the Cambridge-MIT Institute (CMI) and from EPSRC, via a platform grant. The fibres were supplied by Lee Marston and Peter Rooney, of Fibretech, with whom extensive ongoing collaboration is taking place. The authors are also grateful to Andrew Cockburn and Kevin Roberts, of Cambridge University, for assistance with material processing and characterisation.

References

[1] Ducheyne P, Aernoudt E, De Meester P. The mechanical behaviour of porous austenitic stainless steel fibre structures. J Mater Sci 1978;13:2650–8.
[2] Clyne TW, Mason JF. The squeeze infiltration process for fabrication of metal matrix composites. Metall Trans 1987;18A: 1519–30.
[3] Delannay F, Clyne TW. Elastic properties of cellular metals processed by sintering mats of fibres. In: Banhart J et al., editors. MetFoam '99. Bremen, Germany: Verlag MIT Publishing; 1999. p. 293–8.
[4] Yamada Y, Wen CE, Chino Y, Shimojima K, Hosokawa H, Mabuchi M. Processing and mechanical properties of open-cell Mg alloys. Mat Sci Forum 2003;419:1013–8.
[5] Markaki AE, Clyne TW. Mechanics of thin ultra-light stainless steel sandwich sheet material: part I – stiffness. Acta Mater 2003;51(5):1341–50.
[6] Markaki AE, Clyne TW. Mechanics of thin ultra-light stainless steel sandwich sheet material: part II – resistance to delamination. Acta Mater 2003;51(5):1351–7.
[7] Markaki AE, Gergely V, Cockburn A, Clyne TW. Production of a highly porous material by liquid phase sintering of short ferritic stainless steel fibres and a preliminary study of its mechanical behaviour. Comp Sci Techn 2003;63: 2345–51.
[8] Woesz A, Stampfl J, Fratzl P. Cellular solids beyond the apparent density – an experimental assessment of mechanical properties. Adv Eng Mater 2004;6(3):134–8.
[9] Delincé M, Delannay F. Elastic anisotropy of a transversely isotropic random network of interconnected fibres: non-triangulated network model. Acta Mater 2004;52:1013–22.
[10] Markaki AE, Clyne TW. Magneto-mechanical stimulation of bone growth in a bonded array of ferromagnetic fibres. Biomaterials 2004;25(19):4805–15.
[11] Markaki AE, Clyne TW. Magneto-mechanical actuation of bonded ferromagnetic fibre arrays. Acta Mater 2005;53(3): 877–89.
[12] Gibson LJ, Ashby MF. Cellular solids: structure and properties. 2nd ed. Cambridge University Press; 1997.
[13] Olurin OB, Arnold M, Körner C, Singer RF. The investigation of morphometric parameters of aluminium foam using computed micro tomography. Mater Sci Eng A 2002;328: 334–43.
[14] Maire E, Buffiere J-Y, Salvo L, Blandin JJ, Ludwig W, Letang JM. On the application of X-ray microtomography in the field of materials science. Adv Eng Mater 2001;3(8):539–46.
[15] Tan JC, Clyne TW. Analysis of X-ray tomography images of bonded fibre assemblies to measure distributions of fibre segment length and fibre orientation. Acta Mater (Submitted).